Medicon Engineering Themes
Volume 7 Issue 6 December 2024
Article Type: Research Article
ISSN: 2834-7218

Impact Analysis of a Nanosuspension Droplet using Molecular Dynamics

Baiou Shi* and Viet Le

Department of Mechanical Engineering, Penn State Erie, The Behrend College, Erie, PA, USA

***Corresponding Author:** Baiou Shi, Department of Mechanical Engineering, Penn State Erie, The Behrend College, Erie, PA, USA.

Received: October 26, 2024; **Published:** November 26, 2024

DOI: 10.55162/MCET.07.248

Abstract

The behavior of nano-fluids, or fluid suspensions containing nanoparticles in the realm of capillary fluid flow, has garnered tremendous attention recently for applications spanning from household and personal care products to advanced targeted drug therapy and materials fabrication. One concern is how to control the ordering of nano-particle arrays and fabricate those functional devices. Nano-suspension provides us with a path to synthesize and disperse nanoparticles in fluids, however, the fundamental mechanisms about interfaces and wetting kinetics are still unknown when a nanosuspension drop spreads on a solid surface. Herein, results from molecular dynamics simulations will be presented to explore the nanosuspension metal droplet impact process. Furthermore, the results illustrate how the role of impact angle, impact velocity and nanoparticle size affect the spreading kinetics and how this connects dynamic droplet morphology and associated particle positioning on surfaces.

Keywords: Nanosuspension; Droplet Impact; Molecular Dynamics

Introduction

Nanosuspension droplet impact is a common phenomenon integral to many natural and technological processes. Its applications span various fields, including inkjet printing, spray cooling, drug delivery, and oil recovery [1-4], making it crucial to understand the full capabilities of nanodroplet impact. Consequently, extensive research has been dedicated to studying the interactions between nanodroplets and substrates to understand their behavior. When a nanodroplet collides with a solid substrate, it can undergo several different behaviors, including absorption, bouncing, spreading, and fragmentation. Among these, nanodroplet spreading has garnered significant interest. Research has shown that spreading rates are influenced by droplet size, impact speed, surface tension, and viscosity [5-7]. However, uncertainties remain regarding the variables that affect spreading rates, and ongoing research aims to identify and explore the implications of these variables.

The primary interest in nanosuspension droplet spreading stems from its widespread applications. When a nanodroplet spreads upon impact with a substrate, it disperses rather than bouncing or fragmenting. This process can be broken down into three stages: an initial precursor film that moves ahead of the droplet, followed by intermediate and final stages dominated by surface tension and viscous forces [8]. Numerous factors, such as impact angle, surface tension, velocity, electric potential, and nanoparticle size, influence the spreading rate [9-10]. Modifying these variables can alter the behavior, influencing not only spreading speed but also other outcomes like fragmentation, bouncing, or absorption [11-14].

Despite the growing interest in nanosuspension droplet spreading, there are few studies that deeply explore the underlying mechanisms. Most focus on computer simulations to identify potential factors influencing spreading. For instance, Daneshian et al. [11] studied the correlation between impact speed and fragmentation, concluding that at a critical velocity, nanodroplets fragment rather than spreading. Ying Qi et al. [15] investigated the effects of nanoparticle volume and surface wettability, finding that increased volume and wettability reduce the spreading rate. Similarly, Samsonov et al. [16] showed that larger droplets spread more slowly, while Murshed et al. [17] demonstrated that higher Weber numbers also lead to slower spreading. These studies highlight key aspects of nanodroplet spreading and how modifying certain variables influences behavior.

In addition to computational studies, experimental research has provided insights into nanosuspension droplet behavior in real-world applications. These experiments often confirm the findings from simulations [15-17]. For example, Gui et al. [18] found that increasing the number of nanoparticles in a droplet decreases the spreading rate due to increased surface tension. Lui et al. [19] used high-speed cameras to investigate the relationship between nanofluid viscosity and spreading, concluding that higher viscosity suppresses spreading motion. Shen et al. [20] observed that as nanoparticle size increases, spreading rate decreases. These experimental results reinforce the understanding that droplet size, surface tension, and viscosity significantly influence nanosuspension droplet spreading in practical applications.

To contribute to this growing body of knowledge, this paper aims to identify the variables that impact spreading kinetics through two objectives. The first objective is to examine the correlation between impact velocity and nanosuspension droplet spreading and to assess the role of impact angle. This is achieved by simulating the collision of a Cu nanosuspension droplet with a Pb substrate at velocities ranging from 2 to 400 m/s and angles from 30° to 90°. The second objective explores the relationship between nanoparticle size and spreading behavior, varying the size of Cu nanoparticles from the original size to double, with impact angles between 30° and 90° and velocities of 200 and 400 m/s. This study offers valuable insights into the dynamics of nanosuspension droplet spreading, specifically seeks to address key questions regarding the factors that control nanosuspension droplet spreading.

Procedures

Molecular dynamics (MD) simulation employed embedded atom method [21] interatomic potentials for describing interactions between liquid Pb and solid Cu (suspended particles and substrate surfaces). Specific interactions were previously advanced and have been demonstrated to describe this material system with very good accuracy [21-24]. Nonetheless, rather than connecting with a specific material composition, the Cu-Pb system was chosen here based on more general attributes of metallic systems, as described in the preceding section. Liquid metals modeled via EAM potentials typically exhibit relatively high surface tensions γ_{lg} and low viscosity η, in accord with experimental observations on these materials. These quantities were previously computed for the model of Pb (1) used here and at the same $T = 700\ K$ as is modeled here; they are $\gamma_{lg} = 0.574 \pm 0.038\ \mathrm{J/m^2}$ and $\eta = 2 \pm \mathrm{mPa \cdot s}$ [25].

Figure 1 shows two views of typical simulation configuration at time $t = 0$. Fully three-dimensional simulations were employed throughout; however, to reduce the spreading geometry to two dimensions, liquid cylinders were brought into contact with solid surfaces where the length of the cylinder along its axis (i.e. in the y direction) was identical to the periodic dimension of the simulation cell along y (the same was true for the solid surface). Thus, two independent contact lines advanced: one in positive x and another in negative x; results were averaged along y to collapse spreading analyses into the xz plane. Despite this being a model of an infinite length liquid cylinder, the relatively small periodic dimension of the simulation cell along y suppressed Rayleigh instabilities in the liquid while also reducing computational time and permitting study of relatively larger drops. Suspended nanoparticles were also cylinders, akin to what was done with the liquid drop, and it is obvious that they span the simulation in y. Note this is different from recent simulations that also employed cylindrical drops but spherical particles. Here, both spreading and pinning were effectively reduced to two-dimensional (2D) processes, explored via three-dimensional (3D) simulation ensembles.

All results presented here were from isothermal ensembles with T = 700 K, which is ~10% greater than Pb melting point and just over half Cu melting point. The simulation time step throughout was 1 fs and the Molecular Dynamics Simulator LAMMPS was used for all simulations. The solid substrate model was subject to periodic boundary conditions in x and y with the periodic length of the simulation cells L_x ~ 300 nm and L_y ~ 5 nm. Substrate L_x was selected to permit significant droplet spreading without reaching the edge of the simulation cell; L_y was selected as ten times the EAM interaction model cutoff distance. Since spreading (and pinning) are effective 2D processes for the geometry modeled here, this L_y value balances competing desires to have sufficient averaging along the cylindrical axis dimension while also keeping computational cost constrained. Solids were initially equilibrated in fully three-dimensional periodic ensembles at the zero pressure lattice constant and with appropriate unit cell rotation to have either the Cu(001) direction along z. For all equilibration runs, the system was identified to be at equilibrium via temporal analysis of potential energy, pressure, and other system properties. Following the initial bulk solid equilibration, periodic boundary conditions were removed along the z direction, forming two free surfaces for solid substrate. Substrate had thickness in z equal to 5 nm, with ~ 1 nm of thickness at the free surface in the negative z held rigid for all subsequent calculations to prevent system drift in z. To minimize computational expense, L_z was minimized; the value used here permits the presence of a constraining frozen region (as described). Additionally, as described further below, dynamic substrate atoms are portioned along z so that a sufficiently large region of the substrate is subject to a temperature control algorithm, or thermostat, to maintain essentially isothermal spreading. Lastly, a region of substrate atoms in closest proximity to the free surface on which spreading occurs is not subject to thermostat to prevent artificial influences on observed droplet spreading behavior.

Three-dimensional periodic slabs of liquid are equilibrated at the zero-pressure density for the desired T. To reach proper liquid density during equilibration runs, L_x and L_z were allowed to vary while L_y was constant as given by the corresponding substrate's L_y. After liquid slab equilibration, cylinders (with cylindrical axis along y) were extracted from the atomic ensembles and re-equilibrated in free space. Two separate drops were thus formed with nominally identical properties but slightly different L_y. After liquid drop equilibration in free space, the radius of cylindrical drops was determined from plots of number density as a function of radical distance from the cylindrical axis, averaging all data along the cylinder axis in y; the radius was defined as the point on the radial density profile where the plot decreased to half the average density in the bulk liquid. The initial droplet radius was R_0 = 42 nm in all cases studied here; particle insertion into the drops and subsequent re-equilibration (described below) did not change R_0 for particle concentration explored here.

To maintain a three-dimensional simulation geometry but with both spreading and pinning effectively reduced to two-dimensional processes in the xz plane, cylindrical particles were inserted into cylindrical drops. A unique feature to studying particles entrained into the contact line has the capability to drive self-pinning. A cylindrical "particle" was initially extracted from a solid slab used to form a Cu substrate. The nominal extraction radius was ≤ 3 nm; copies of this model particle were then inserted into the drop in multiple, random locations. Particle size was chosen somewhat heuristically to be approximately one-tenth of the modeled droplet size. Insertion was done so as to ensure that all atoms in a given inserted particle were outside the interaction range of atoms in other particle at t = 0; furthermore, particles inserted near the drop edge required to have at least 75% of the particle's volume inside the drop. To insert a particle, a cylinder of liquid atoms was extracted from the drop using a radial cutoff around the determined insertion point; the cutoff was chosen to ensure that, upon merging a copy of the particle into the drop, the closest separation distance between a drop atom and a solid particle atom was equal to the equilibrium separation distance observed at planar solid-liquid interfaces for this system [26]. After the desired number of particles was inserted, nanosuspension drops were re-equilibrated in free space. Within a few tens of picoseconds after starting these simulations, a small number of particle atoms rapidly developed facets on low index crystallographic planes. Equilibration of nanosuspension drops was thus relatively quick, relative to simulation time scales. After faceting, following equilibration, the particle radius was r ≤ 3 nm. Also, in considering the effects of particle sizes, Cu particles with twice the size were inserted at the same locations.

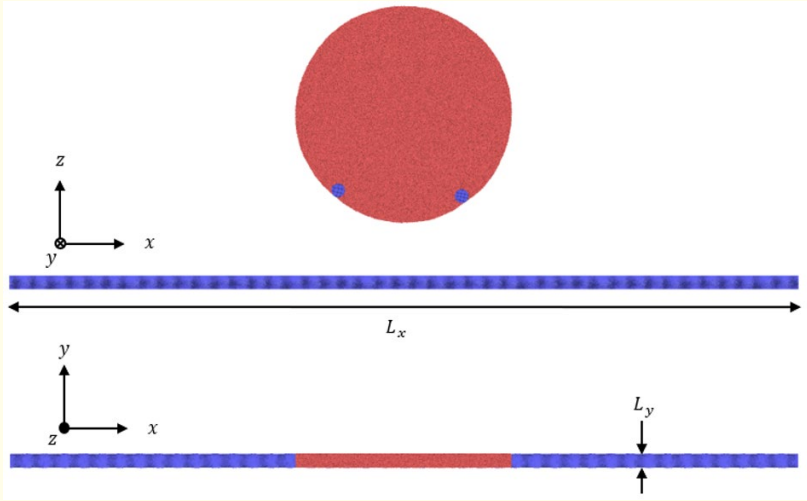

Figure 1: Two orthographic projection views of a simulation configuration at $t = 0$ (Pb atoms are red; Cu atoms are blue). The image is for a $R_0 = 42$ nm drop with 2 Cu particles in contact with the (001) surface of Cu. The spreading direction is x, the free surface normal direction is z, and the droplet's (and particles') cylindrical axes are along y. The periodic repeat lengths of the simulation cells are $L_x = 300$ nm and $L_y = 5$ nm; graphics are rendered using OVITO.

In this study, the cylindrical droplets with inserted particles were suspended above the solid substrate at 2 nm and 20 nm. The liquid droplets were initialized a velocity of 2 m/s, 20 m/s, 200 m/s, and 400 m/s using LAMMPS to simulate an impact contact. The impact angles were also varied from 30°, 45°, 60° to 90°. The angles were defined with respect to the x axis: a 90° impact angle represents the droplets impact perpendicularly to the substrate and a 0° impact angle describes the droplet moving parallel to the x axis.

Results and Discussion

Effect of impact velocity on the spreading of the droplet

To characterize wetting kinetics, the extent of spread versus time is shown in Fig. 2 with Pb liquid droplet with two suspended Cu particles impacting on the Cu(001) surface. Data were obtained from the edge of the drop, making certain to compute the edge position above the two-layer precursor film observed to form in these systems. Therefore, wetting data indicated droplet spreading and not precursor film advancement. For all the impacting simulations in Fig. 2, the initial position of droplet was set to be 2 nm above the Cu substrate. We compared four different runs in Fig. 2 with various impact velocities of 2 m/s, 20 m/s, 200 m/s, and 400 m/s, but with the same impact angle of 90°, which means droplet is perpendicular to the solid substrate at $t = 0$. Due to the various impact velocities, time that spent for the droplet to contact the substrate also varies. For instance, considering the slowest speed of 2 m/s in Fig. 2, droplet took about 0.7 *ns* to impact the Cu substrate. As a common observation for low viscosity, high wettability liquids, wetting of Pb(l) on Cu(001) is initially characterized by an inertial wetting regime of very rapid spreading. This is followed by a slower spreading regime wherein dynamics are governed by viscous effects and/or contact line phenomena. The same trend is shown in Fig. 2 that all the curves begin with a steeper slope and then as the contact line velocity slows down, spreading goes towards the second regime as the curve becomes less steeper. However, the impacting velocity does influence the wetting kinetics. As shown in Fig. 2, the Pb droplet with impacting velocity of 400 m/s exists the fastest spreading upon contacting the Cu(001) surface. This is due the highest kinetic energy associated with the droplet of the largest impacting speed.

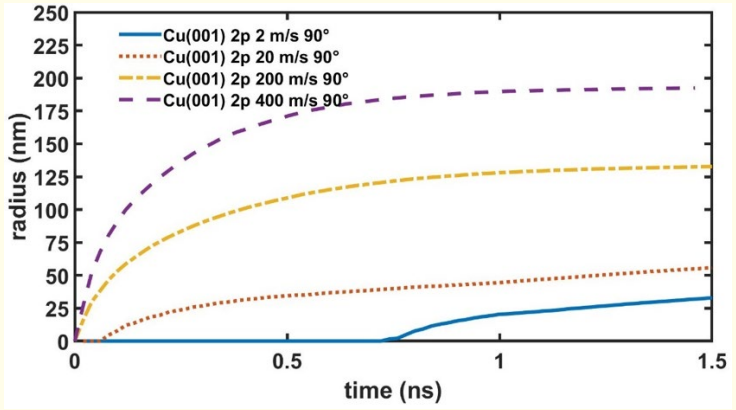

Figure 2: Extent of droplet spread in the *x* direction at an impact angle of 90° and at 4 different velocities of 2 m/s, 20 m/s, 200 m/s, and 400 m/s.

In Fig. 3, the extent of the droplet at left and right side of the subtrate was plot against time. Two simulations were run at an impact angle of 45° and at two initial velocities of 400 m/s and 200 m/s. In two runs, the droplets were suspended 20 nm above the subtrate. After impacting the subtrate, the droplets spread along the *x* axis. Distance from the instantaneous center of mass of the droplet to the leftmost and rightmost, named left and right radius respectively, was analyzed. In this case, the impact angle was changed to 45°, the 400 m/s droplets showed a faster spreading rate for both left and right sides. In both runs, the left radius is spreading further than the right radius. When the droplet impacting at 45°, the horizontal component of velocity created a momentum and pushed the droplet to the right. Because the radius analysis was calcualted using instantaneous center of mass of the droplet, as the spreading was proceeding, the center of mass of the droplet was sided to the right and getting further from the left edge. Hence, the extent of left side of the droplet is further than that of the right sides.

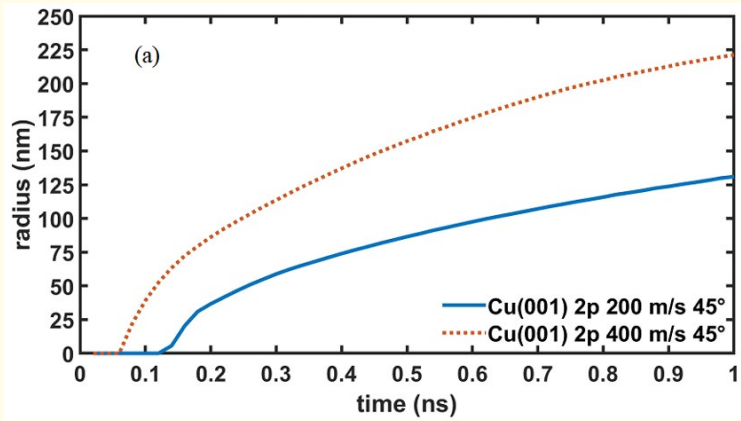

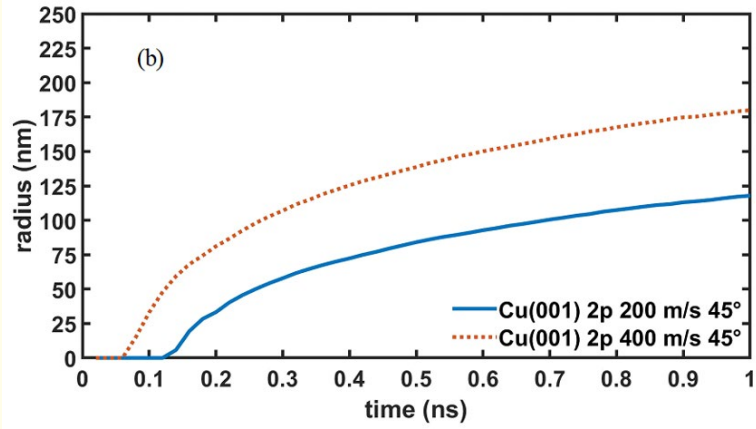

Figure 3: (a) Extent of droplet spread in the left side of the *x* direction at 200 m/s and 400 m/s at an impact angle of 45° (b) Extent of droplet spread in the right side of the *x* direction at 200 m/s and 400 m/s at an impact angle of 45°.

Effect of contact angle on the spreading of the droplet

The extent of spreading of liquid droplet with two inserted regular size particles upon impacting the solid subtrate versus time was shown in Fig 4. Data from a run with a Pb droplet without inserted particles (pure droplet) was collected and also presented in this figure. With these five simulations, the droplets were suspended 20 nm above the subtrate and had a same initial velocity of 200 m/s. The impact angles were varied at 30°,45°,60° and 90° to investigate effects of impact angle on droplet spreading behaviors. These angles were set with respect to negative *x*-axis. Both the left and right radius were shown in Fig 4. Observing from the plots, with a larger impact angle, the droplet was approaching the solid substrate at faster speed, which reflected in the impact time. For instance, shown in Fig. 4b, the droplet hit the solid subtrate around 0.1 ns in 60° run, while in 30° run, the droplet did not impact the substrate until 0.085 ns later. This is justifiable, because the vertical component of initial velocity is larger at a higher angle. From two plot, the spreading rate of a droplet with two inserted solid particles and a pure droplet showed no substantial differences at inerial wetting regime. However, at a slower spreading regime, the pure droplet took over the inserted particles droplet. This can be explained by the particles pin to the substrate and slow down the spreading. In Fig. 4a, the extent of the droplet left side converged to around 125 nm. While in Fig. 4b, the right extent of the droplet were still spreading at different rates. Though same converging behavior is expected. With a higher impact angle, the horizontal momentum of the droplet is smaller, therefore they slowed down much faster. The horizontal momentum in the droplet retains much longer at right side due to much of the horizontal momentum distributed to the positive *x* direction or the right side.

Fig. 5 illustrates the extent of spreading of Pb droplet with two inserted regular size solid particles versus time from data of five simulations. In these five runs, the droplet was susppended 20 nm above the subtrate and had various impact angles ranging from 30°,45°,60° and 90°. Data from a run with a Pb droplet without inserted particles (pure droplet) was collected and also presented in this figure. However, in these five run, the droplet was experiencing a high inintial velocity in expericing. Like previous figure, the data of extent of droplet spreading along the *x* axis at left and right sides are being analyzed. Similar behavior of droplet spreading also exihibits in these five run. Even with high impact velocity, i.e. 400 m/s, a larger impact angle exhibits a higher speading rate. This shows a consistenct effects of changing in impact angle.

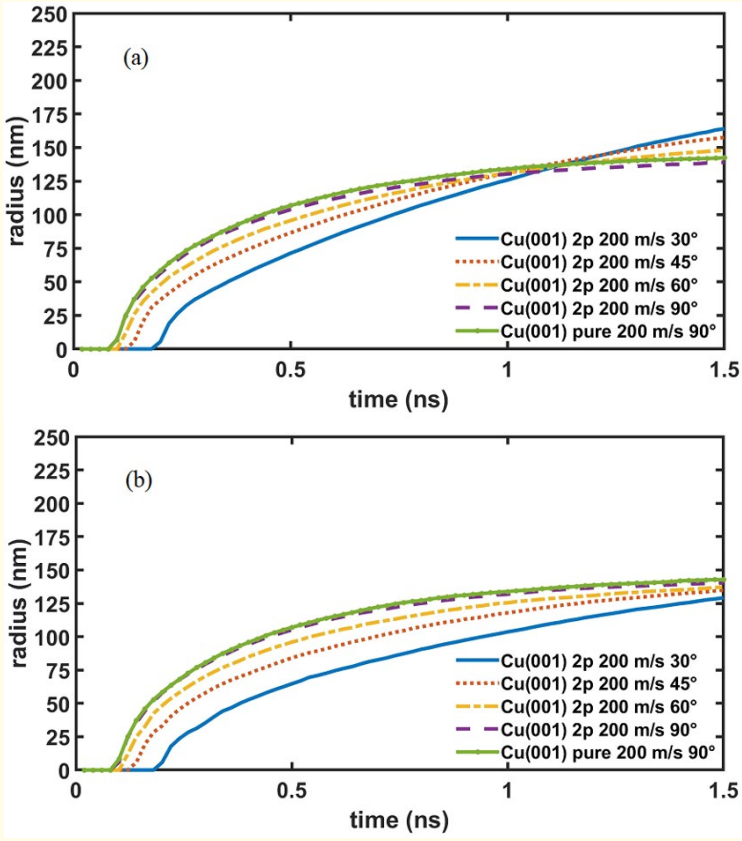

Figure 4: (a) Extent of droplet spreading in the left side of the *x* direction at 30°,45°,60° and 90° and 200 m/s; (b) Extent of droplet spread in the right side of the *x* direction at 200 m/s.

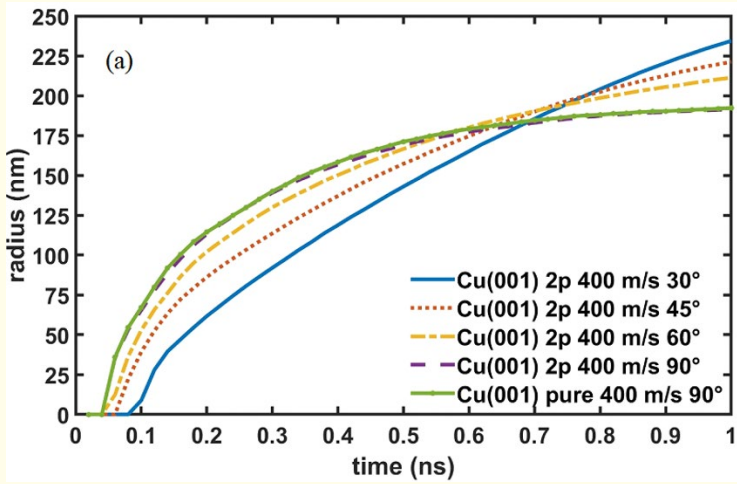

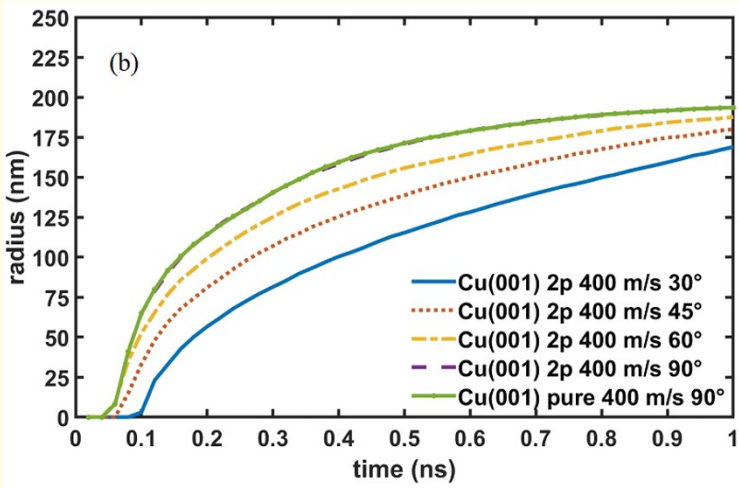

Figure 5: (a) Extent of droplet spread in the left side of the *x* direction 30°, 45°, 60° and 90° and at 400 m/s; (b) Extent of droplet spread in the right side of the *x* direction at various angle and at 400 m/s.

Effect of particle size on the spreading of the droplet

The characterization of wetting kinematics and droplet size is displayed in Fig. 6 with Pb liquid droplet with two suspended Cu nanoparticles with varying sizes impacting on the Cu(001) surface. Cu nanoparticles in Fig. 6 vary from original size (~ 3nm) to double size (~ 6nm), Which is intended to identify the influence that size of nanoparticle has on the overall spreading of the droplet. Data were obtained from the edge of the drop, making certain to compute the edge position above the two-layer precursor film observed to form in these systems.

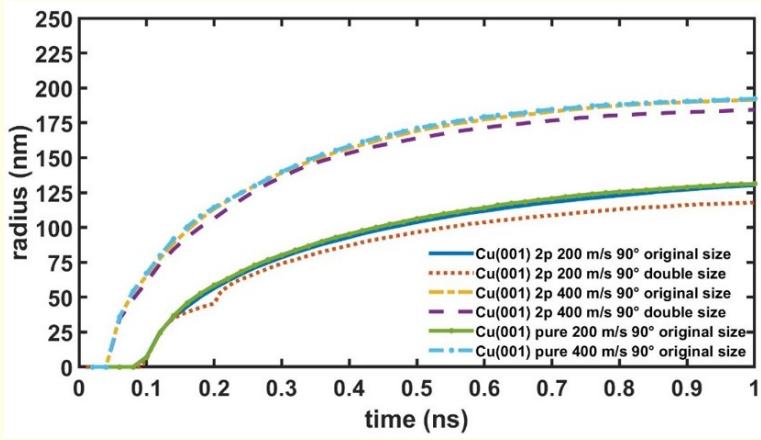

Figure 6: Extent of droplet spread in the *x* direction at two different particle sizes and two impact speeds with an impact angle of 90°.

For all the impacting simulations in Fig. 6, the initial position of the droplet was set to be 20 nm above the Cu substrate. Fig. 6 compares six different runs with varying amounts of nanoparticles of two and zero particles, nanoparticle size of original and double size, and impact velocity of 200 m/s and 400 m/s at an impact angle of 90. Based on the visual representation of the radial spreading of each nanodroplet run, two distinct spreading curves were formed. The first curve is composed of three-run with 400 m/s impact velocity. These runs reach a radial spreading of 180 to 195 nm in 1 ns, which demonstrates that nanodroplet spreading is largely influenced by the impact velocity. However, within the first curve there a discrepancy between the three runs. As time progresses in the first curve the run starts very minusculely deviate from each other. The pure Cu(001) spreads the quickest, showing that the inclusion of nanoparticles in a droplet inhibits the fluidity of the nanosuspension droplet. Then, the double-sized 2 nanoparticle Cu(001) spreads at the slowest pace in the first curve, conveying the notation that increasing the nanoparticle size impedes the spreading motion. These observations are more pronounced in the second curve. The second curve is comprised of three runs at impacts velocity of 200 m/s, and each run takes a 1 ns to reach a radial spreading of 117-140 nm. This drastically increases in spreading time, expresses the idea that impact velocity has a tremendous effect on the spreading rate of a nanodroplet. As aforementioned, the remarks of the first curve are more displayed on the second curve, especially the affect nanoparticle size. In the second curve, the doubled nanoparticle size greatly reduced the spreading rate of the nanodroplet in comparison to the other two runs. This correlation of nanoparticle inclusion and size on the spreading rate is due to the surface tension. As the nanoparticles are added or their sizes increase, the nanodroplet's surface tension intensifies and slows the spreading rate of the nanosuspension droplet.

At impact angle of 30°

The relation of nanoparticle size and radial spread is represented in Fig. 7 with a Pb liquid droplet containing two Cu nanoparticles with varying sizes impacting the Cu(001). Cu nanoparticles size in Fig. 7 range from an original size (~ 3nm) to double size (~ 6nm), to compare the effects of nanoparticle size on the overall nanodroplet spreading. For both simulations runs, the nanosuspension droplet is 20 nm above the Cu(001) substrate and impacts the substrate at 400 m/s at an angle of 30 degrees (from the positive x-axis). Using the data from those runs Fig. 7 is constructed, portraying the radial spreading behavior of the nanodroplet via time. In Fig. 7a, the aftermentioned behavior is displayed through the perspective of the droplet spreading on the left side of x direction, and for Fig. 7b the perspective is of the right side of the x direction.

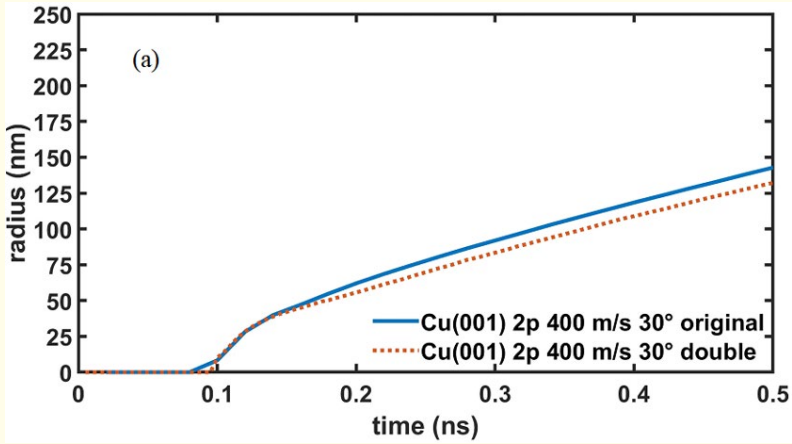

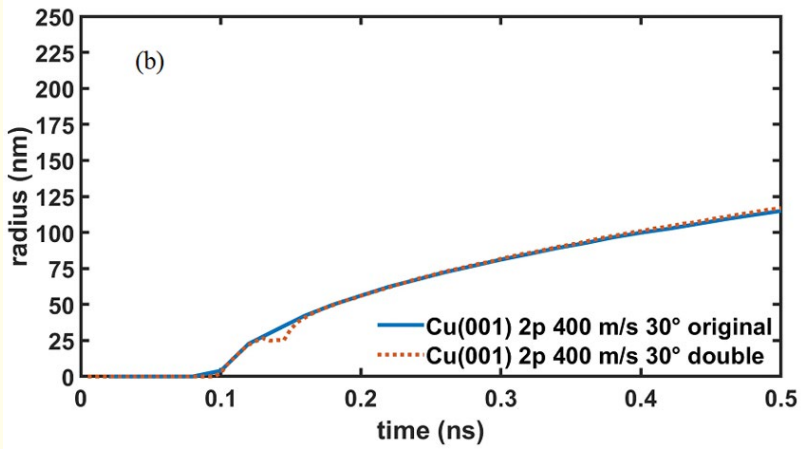

Figure 7: (a) Extent of droplet spread in the left side of the *x* direction at two different size and at 400 m/s and 30° impact angle; (b) Extent of droplet spread in the right side of the *x* direction at two different size and at 400 m/s and 30° impact angle.

In Fig. 7a, the orginal size and double size runs reaches a radial spreading of 152 and 132 nm respectively in 0.5 ns. Each run had followed the same beginning path, until roughly 0.15 ns where they started to diverge. The run with double-sized nanoparticles at roughly 0.15 ns stated to spread at a slower velocity than the original size nanoparticles. Presenting the idea that as the size of nanoparticle increases the overall velocity of the radial spreading will decrease.

In Fig.7b, the orginal size and double size runs reaches a radial spreading of 116 and 120 nm respectively in 0.5 ns.. Each run followed nearly identical spreading paths, except for the double size run had a deviation roughly at 0.15 ns. However, the nanodroplet returned to the original runs spreading curve. Arising the idea that impact velocity in x-direction affects the spreading behavior of the opposite side of the impact angle, and nanoparticle size doesn't effect it.

At impact angle of 45°

The association of nanoparticle size and radial spreading at a certain impact angle is portrayed in Fig. 8 with a Pb liquid droplet containing two Cu nanoparticle with ranging sizes impacting a Cu(001) substrate. The two nanoparticle's sizes are an original (~ 3nm) and a double (~ 6nm) For each run, the nanodroplet is 20 nm above the Cu(001) substrate and impacts it at 400 m/s at 45 degrees(-from the positive x-axis). Utilizing the simulation data, Fig. 8 was constructed to visually represent the behaviors that nanodroplet exhibits. In Fig. 8a the droplet's spreading behavior is illustrated from the viewpoint of the left side of the x direction, and in Fig. 8b it's from the right.

In Fig. 8a the orginal size and double size runs reaches a radial spreading of 154 and 142 nm respectively in 0.5 ns. Each run had an identical initial spreading, however, when the runs reached 0.1 ns, they diverged from each other. The double size nanoparticle run had a slower radial spreading in relation with time than the original size nanoparticle. Indicating that the double-sized nanoparticle simulation experienced lower velocity in comparison two the original sized nanoparticle run, and thus a more inhibited spreading fluidity.

In Fig. 8b each run had the nanodroplet spread to 138 nm in 0.5 ns. Both runs followed an identical path with little no deviation. This representation is almost indistinguishable from Fig. 7b graph. Resulting in the observation that nanodroplet spreading behavior on the opposite side of x direction of impacts is governed by the impact angle and impact velocity, but not nanoparticle size.

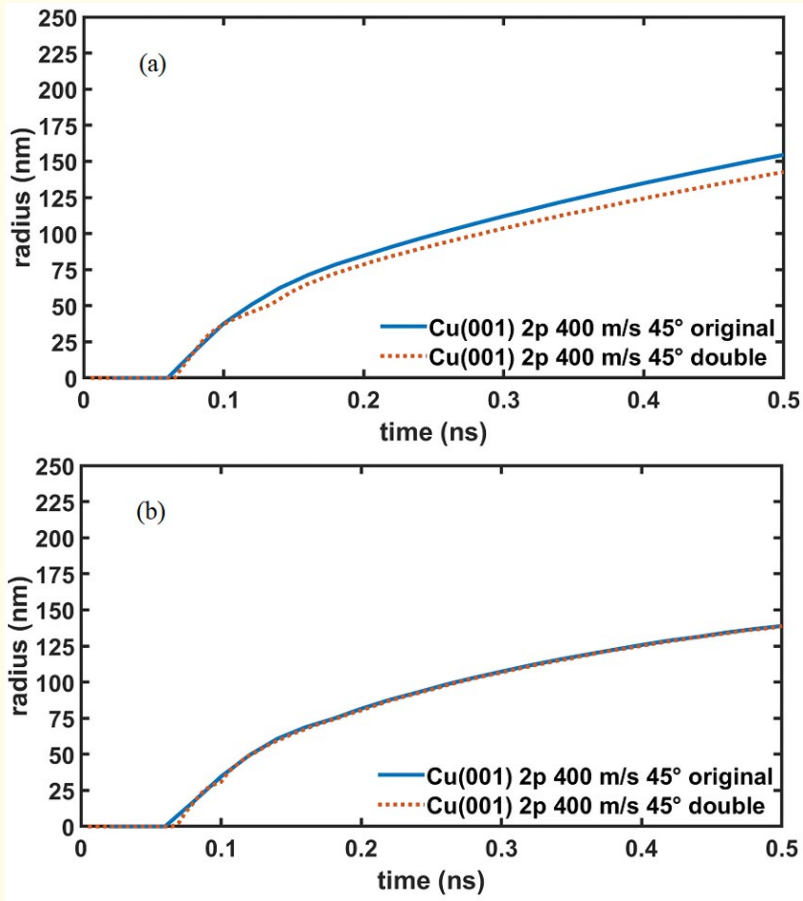

Figure 8: (a) Extent of droplet spread in the left side of the *x* direction at two different size and at 400 m/s and 45° impact angle; (b) Extent of droplet spread in the right side of the *x* direction at two different size and at 400 m/s and 45° impact angle.

At impact angle of 60°

The connection of nanoparticle size and radius spreading at a particular impact angle is displayed in Fig. 9 using a Pb liquid droplet containing two Cu nanoparticles at different sizes impacting a Cu(001) substrate. For each of the simulation runs, the nanodroplet impacts the substrate at 400 m/s at an angle of 60 degrees. Just like the two previous figures, the simulation data was displayed in Fig. 9 with Fig. 9a being the left side and Fig. 9b being the right side.

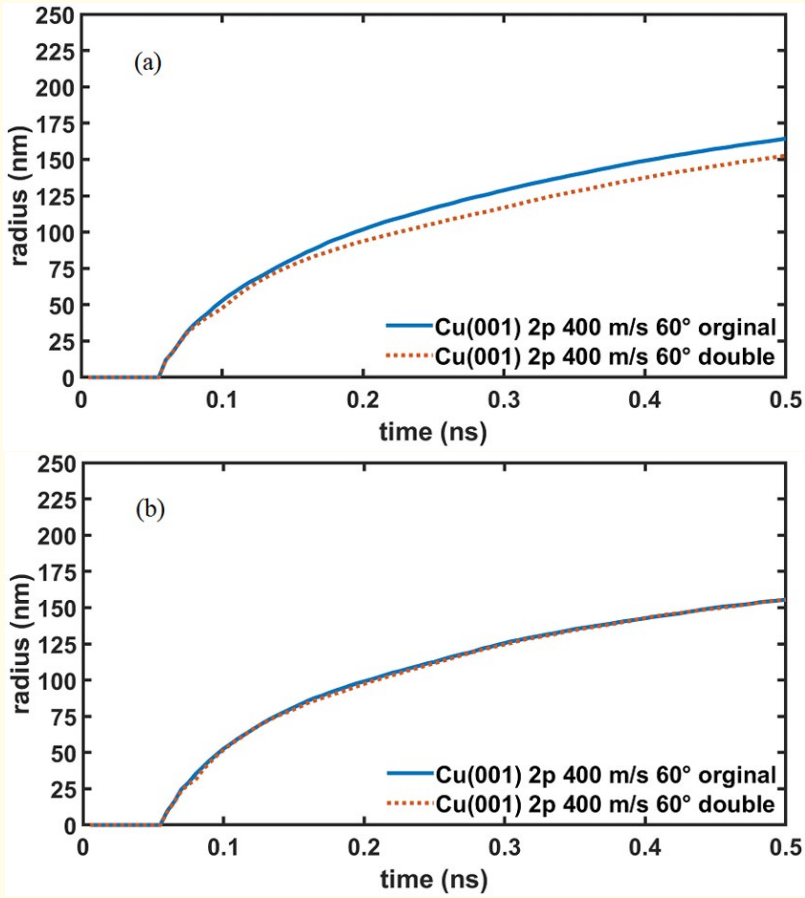

Figure 9: (a) Extent of droplet spread in the left side of the *x* direction at two different size and at 400 m/s and 60° impact angle; (b) Extent of droplet spread in the right side of the *x* direction at two different size and at 400 m/s and 60° impact angle.

In Fig. 9a the original size run reaches 164 nm radial spreading in 0.5 ns, while the double-sized run reaches 152 nm in roughly 0.5 ns. This disparity in the spreading distance is greatly amplified in comparison with Fig. 7a & 8a, arising the question of why. The separation is due to the increase of nanoparticle size inhibiting the speed of spreading. However, when compared to the other figures (7a & 8a) it noticeable that the impact angle affects the radial spreading. As the impact angle increases the droplet is spreading at a faster rate, since Fig. 7a the nanodroplet spread to 125 nm in 0.5 ns, and Fig. 8a spreads to 150 nm in 0.5 ns, but Fig. 9a reaches 150 nm in 0.4 ns. For Fig. 9b, the original size run reaches 155 nm in 0.5 ns and the double reach 155 nm in 0.5 ns. Similar to Fig. 7b and 8b, both runs follow the same path due to the fact impact velocity in the x-direction are equivalent in both runs. The double size nanoparticle spreads at a lower amount because of the nanoparticle size prohibits the nanoparticle to spread freely.

At impact angle of 90°

Similar to Fig. 7, 8, & 9, the effect of nanoparticle size and radial spread was charted in Fig. 10 with a Pb liquid droplet with two different sized Cu nanoparticles impacting a Cu(001) substrate. In all the simulation, the nanodroplet is impacting the substrate at 400 m/s at an angle of 90 degrees, directly above the substrate. Similar to the previous figures, Fig. 10 is composed of two plots, plot a is the left side of the radial spreading and plot b is the right side.

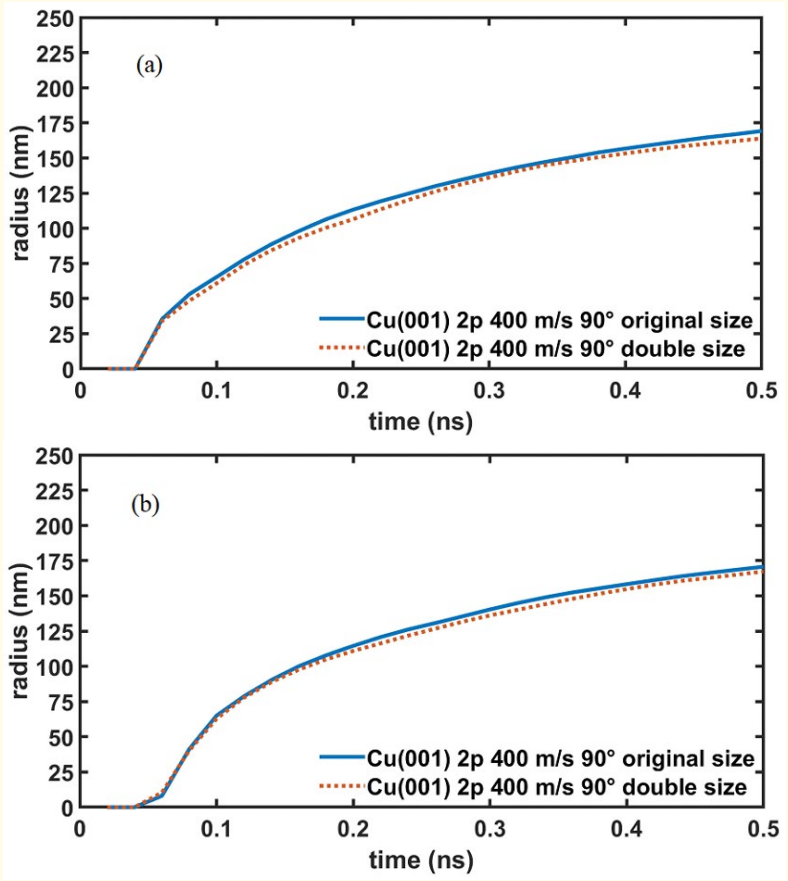

Figure 10: (a) Extent of droplet spread in the left side of the *x* direction at two different size and at 400 m/s and 90° impact angle (b) Extent of droplet spread in the right side of the *x* direction at two different size and at 400 m/s and 90° impact angle.

In Fig. 10a and 10b. each run reached a radial spreading of 160 to 170 nm in roughly 0.5 ns. For each of the two plots, the double nanoparticle size curve had a slower velocity of spreading. Indicating that as nanoparticle size increases the spread rate decreases, which was similar to Fig. 7-9. Also, when comparing the results of Fig. 7-10 a clear trend occurs. As impact angle increases from 30-90 degrees, the nanodroplet has a larger horizontal spreading velocity causing to spread to the limits of the simulation box in a shorter period. Coupled with nanoparticle size observations, solidifies the notation that to achieve fast spreading rate, the ideal configuration is to directly place the nanodroplet 90 degrees from the substrate and have a small nanoparticle size inclusion in the droplet. This allows the nanodroplet to experience a uniform velocity that causes the droplet to spread evenly along each side of the substrate and has a lower amount of impendence in the fluidity of spreading by the nanoparticles.

Conclusion

This study offers valuable insights into the dynamics of nanosuspension droplet spreading, specifically concerning the effects of nanoparticle size, impact velocity, and impact angle. Using molecular dynamics simulations, we demonstrated that the spreading kinetics of a Cu nanosuspension droplet impacting a Pb substrate are significantly influenced by both velocity and angle. Higher impact velocities, such as 400 m/s, led to faster and more extensive droplet spreading due to increased kinetic energy, while larger impact

angles resulted in quicker substrate contact and a distinct distribution of horizontal momentum. Additionally, the simulations showed that the presence of nanoparticles within the droplet had little effect on the initial spreading phase but hindered later stages due to particle pinning effects.

In 3D simulations, we analyzed radial spreading in the x-direction across various configurations of impact velocity, impact angle, and nanoparticle size. The first objective examined the relationship between impact velocity and angle on radial spreading, varying the nanoparticle quantity (0 or 2), impact velocity (200 to 400 m/s), and impact angle (30°, 45°, 60°, and 90°). The second objective investigated how nanoparticle size influences spreading rate by comparing droplets with nanoparticles ranging from original to double size under the same range of velocities and angles. Data were plotted as radial spreading versus time graphs, revealing the progression of each simulation and the impact of each variable on droplet spreading.

For the first objective, the simulations clearly demonstrated that impact velocity, angle, and nanoparticle quantity have a significant effect on nanosuspension droplet spreading. The data showed a positive correlation between impact velocity and radial spreading. For example, increasing the velocity from 200 to 400 m/s resulted in faster droplet spreading due to greater horizontal momentum. At lower impact velocities, the spreading was uneven, with faster spreading in the negative x-direction and slower spreading in the positive x-direction. This behavior reversed at higher impact angles due to the horizontal momentum distribution. At higher velocities, droplet spreading became more uniform across all angles, with larger angles producing faster spreading. Nanoparticle quantity also had a noticeable effect: droplets with no nanoparticles spread faster than those with two, suggesting that more nanoparticles hinder fluidity and limit the spreading rate.

For the second objective, the effect of nanoparticle size on droplet spreading was more nuanced. When droplets with double-sized nanoparticles impacted the substrate perpendicularly at 90°, they spread more slowly in both x-directions compared to those with original-sized nanoparticles. However, at lower angles, while the negative x-direction spread was slower for larger nanoparticles, the positive x-direction spreading rate remained the same. This behavior is attributed to the distribution of nanoparticles upon impact, where nanoparticles tend to follow the droplet's impact trajectory, concentrating more on the negative *x*-axis side. Ultimately, the findings suggest that larger nanoparticle sizes negatively correlate with radial spreading.

These results enhance our understanding of nanosuspension wetting behaviors, which are critical in applications such as materials fabrication and targeted drug delivery. The observed influence of impact velocity, angle, and nanoparticle size on spreading dynamics paves the way for optimizing droplet behavior in various technological applications. Future research should explore more complex interactions, focusing on factors like interatomic potential energy, material composition, and how different conditions induce behaviors such as absorption, bouncing, or fragmentation. This could help refine the control of nanosuspension droplet spreading for practical applications, making these droplets more accessible for real-world use.

References

1. Son Y., et al. "Spreading of an Inkjet Droplet on a Solid Surface with a Controlled Contact Angle at Low Weber and Reynolds Numbers". Langmuir 24.6 (2008): 2900-2907.
2. Chakraborty S., et al. "Thermo-physical properties of Cu-Zn-Al LDH nanofluid and its application in spray cooling". Applied Thermal Engineering 141 (2018): 339-351.
3. Kumar A, Zhang X and Liang X. "Gold nanoparticles: Emerging paradigm for targeted drug delivery system". Biotechnology Advances 31.5 (2013): 593-606.
4. Peng B., et al. "A review of nanomaterials for nanofluid enhanced oil recovery". RSC Advances 7.51 (2017): 32246-32254.
5. Cordeiro J and Desai S. "The Effect of Water Droplet Size, Temperature, and Impingement Velocity on Gold Wettability at the Nanoscale". Journal of Micro and Nano-Manufacturing 5.3 (2017).
6. Chen H, Nie Q and Fang H. "Many-body dissipative particle dynamics simulation of Newtonian and non-Newtonian nanodroplets spreading upon flat and textured substrates". Applied Surface Science 519 (2020): 146250.

7. Goede TC., et al. "Predicting the maximum spreading of a liquid drop impacting on a solid surface: Effect of surface tension and entrapped air layer". Physical Review Fluids 4.5 (2019).
8. Sedighi N, Murad S and Aggarwal SK. "Molecular dynamics simulations of spontaneous spreading of a nanodroplet on solid surfaces". Fluid Dynamics Research 43.1 (2010): 015507.
9. Gennes PG. "Wetting: Statics and dynamics". Reviews of Modern Physics 57.3 (1985): 827-863.
10. Bonn D., et al. "Wetting and spreading". Reviews of Modern Physics 81.2 (2009): 739-805.
11. Daneshian B and Assadi H. "Impact Behavior of Intrinsically Brittle Nanoparticles: A Molecular Dynamics Perspective". Journal of Thermal Spray Technology 23.3 (2013): 541-550.
12. Gao S., et al. "Nanodroplets Impact on Rough Surfaces: A Simulation and Theoretical Study". Langmuir 34.20 (2018): 5910-5917.
13. Rasih RA, Sidik NA and Samion S. "Recent progress on concentrating direct absorption solar collector using nanofluids". Journal of Thermal Analysis and Calorimetry 137.3 (2019): 903-922.
14. Jaques YM and Galvão DS. "Spreading patterns of high velocity nanodroplets impacting on suspended graphene". Journal of Molecular Liquids 292 (2019): 110429.
15. Li Y., et al. "Nanoparticle-tuned spreading behavior of nanofluid droplets on the solid substrate". Microfluidics and Nanofluidics 18.1 (2014): 111-120.
16. Samsonov VM, Zhukova NA and Dronnikov VV. "Molecular-dynamic simulation of nanosized droplet spreading over a continual solid surface". Colloid Journal 71.6 (2009): 835-845.
17. Murshed SM and Castro CA. "Spreading Characteristics of Nanofluid Droplets Impacting onto a Solid Surface". Journal of Nanoscience and Nanotechnology 11.4 (2011): 3427-3433.
18. Lu G and Lu G. "Experimental Study on the Nanofluid Dynamic Wetting". Dynamic Wetting by Nanofluids (2016): 23-40.
19. Liu HL., et al. "Spreading behaviors of high-viscous nanofluid droplets impact on solid surfaces". Korea-Australia Rheology Journal 31.3 (2019): 167-177.
20. Shen J., et al. "Single Droplet Impingment: Effect of Nanoparticles". Proceedings of the ASME 2008 Fluids Engineering Division Summer Meeting collocated with the Heat Transfer, Energy Sustainability, and 3rd Energy Nanotechnology Conferences. Volume 2: Fora. Jacksonville, Florida, USA. ASME (2008): 621-628.
21. Foiles SM, Baskes MI and Daw MS. "Embedded-atom-method functions for the fcc metals Cu, Ag, Au, Ni, Pd, Pt, and their alloys". Phys. Rev. B Condens Matter 33.12 (1986): 7983-7991.
22. Lim HS, Ong CK and Ercolessi F. "Stability of face-centered cubic and icosahedral lead clusters". Surface Science 269-270 (1992): 1109-1115.
23. Hoyt JJ., et al. "An embedded atom method interatomic potential for the Cu-Pb system". Modeling and Simulation in Materials Science and Engineering 11.3 (2003): 287-299.
24. Webb EB., et al. "Atomistic simulations of reactive wetting in metallic systems". Journal of Materials Science 40 (2005): 2281-2286.
25. Webb EB and Shi B. "Early stage spreading: Mechanisms of rapid contact line advance". Current Opinion in Colloid and Interface Science 19.4 (2014): 255-265.
26. Palafox-Hernandez JP, Laird BB and Asta M. "Atomistic characterization of the Cu-Pb solid-liquid interface". Acta Materialia 59.8 (2011): 3137-3144.

Volume 7 Issue 6 December 2024